Research Article

Yuhai Wang, Chunxu Wang*, Yongling Zhang, Jia Wang, and Li Wang

Preparation of silver nanosheet-assembled film as a surface-enhanced Raman scattering substrate

https://doi.org/10.1515/revac-2022-0047 received June 29, 2022; accepted September 10, 2022

Abstract: In this work, we demonstrate a simple method for the fabrication of silver (Ag) nanosheet-assembled film on aluminum (Al) foil based on the galvanic displacement reaction between Al and Ag+. In order to obtain Ag nanosheets with large area and high aggregation density, both F⁻ and H⁺ ions were introduced into the reaction system to etch the barrier layer Al₂O₃ on Al foils and promote the increase of the number of Ag nuclei. Therefore, Ag nuclei grew into nanosheets with citrate ions as the shape control agent. By varying the reaction parameters, Ag nanosheet film was optimized for surface-enhanced Raman scattering (SERS) measurements. The Ag nanosheet film prepared by the presented method exhibit the advantages of controllable morphology, good SERS activity, and distribution in large area, which could be utilized as a promising SERS-active candidate substrate for analytical applications.

Keywords: Al foil, galvanic displacement, Ag nanosheets, surface-enhanced Raman scattering

1 Introduction

Surface-enhanced Raman scattering (SERS) spectroscopy is a highly sensitive and useful analytical technique, which has been considered to have great potential in various research fields, such as materials chemistry, analytical chemistry, and biology [1–7]. Many studies have shown that when SERS substrates have outstanding enhancement performance, they can be used to detect analytes at very

Yuhai Wang, Yongling Zhang, Jia Wang: College of Information Technology, Jilin Normal University, Siping, 136000, China Li Wang: College of Chemistry, Jilin Normal University, Siping, 136000, China low concentrations [8,9]. It is well known that the neighboring nanoparticles are so close that they form gaps with an ultrahigh electromagnetic field, which are called "hot spots" that provide a possibility for detecting trace molecules even single molecule [10,11]. For highly sensitive SERS detection, various kinds of SERS substrates have been fabricated successively, such as metal electrodes [12–14], island films [15,16], nanoparticles [17,18], and ordered nanostructures [19–21].

Compared with physical methods, chemical methods have obvious advantages for the fabrication of SERS-active substrates, such as noble materials, low-cost, and simple processes. The galvanic displacement reaction is an attractive chemical method that can fabricate nanostructure on solid supports. It is a typical electroless deposition that takes place in solution. The electrical potential difference between the cathode and anode is the driving force for the reaction. For example, the Ag⁺/Ag pair has higher redox potential (0.80 V vs standard hydrogen electrode (SHE)) than Cu^{2+}/Cu , Al^{3+}/Al and Zn^{2+}/Zn pairs (0.34, -1.67, and -0.762 V vs SHE, respectively) [22–25]. Ag nanodendrites can be prepared by the galvanic displacement reaction of elemental Cu, Al, and Zn with Ag⁺ in plating solution [26–30]. High electromagnetic fields are generated at overlapped branches and tips of the branches, so the dendrites have good SERS activity [22,28,29,31]. However, the reaction rate is usually fast, and the generated Ag dendrites fall off easily because of weak adhesion between the dendrites and the substrates, which is a great inconvenience for SERS experiments. Nanosheets assembled on some substrates such as Cu and Si are also common structures [32–34]. For metal Al, when it reacts with Ag⁺ in solution, reaction Eq. 1 usually occurs but not react in Eq. 2. A thin oxide layer Al₂O₃ is formed on the surface of Al foil, which stops further galvanic displacement reaction. To overcome the obstacle, F⁻ is has been introduced into the reaction system. According to the reaction in Eq. 3, the Al₂O₃ layer is etched and forms soluble AlF₆³⁺; thus, Al and Ag⁺ could react continually in accordance with the reaction in Eqs. 2 and 4 [22,26].

^{*} Corresponding author: Chunxu Wang, College of Information Technology, Jilin Normal University, Siping, 136000, China, e-mail: wangchunxujlnu@126.com

Anodic:

$$2Al + 3H2O - 6e \rightarrow Al2O3 + 6H+,$$
 (1)

$$Al - 3e \rightarrow Al^{3+}$$
. (2)

Alumina dissolution:

$$Al_2O_3 + 6H^+ + 12F^- \rightarrow 2AlF_6^{3-} + 3H_2O.$$
 (3)

Cathodic:

$$Ag^+ + e \rightarrow Ag.$$
 (4)

In this work, we report a facile method for fabricating Ag nanosheets by the galvanic displacement reaction of commercial Al foil with AgNO3. For this aim, NaF was introduced into the reaction for etching Al₂O₃. To promote the formation of Ag⁺ nanosheets, trisodium citrate was employed as a shape-controlling agent in the reaction. But trisodium citrate is a salt of a weak acid, and it can reduce H⁺ in solution. This is not conducive to the dissolution of Al₂O₃ on Al foils. Therefore, HNO₃ was added to compensate for the lack of H⁺ in the solution. All Ag nanostructures prepared in this experiment have very good resistance to washing. Even if the reaction time lasted up to 2h, the Ag nanostructures did not peel off from the surface of Al foils. More importantly, by altering the experimental conditions, the morphology of the nanostructures was adjustable, and they presented tunable and good enhancement ability for SERS applications.

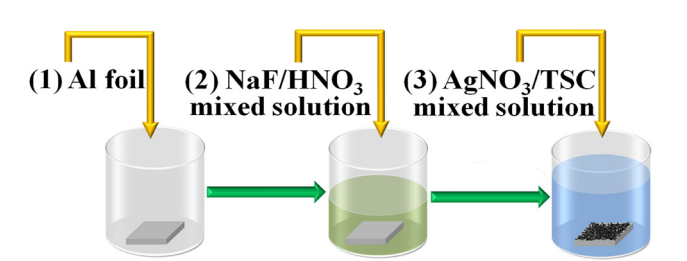
2 Materials and methods

2.1 Materials

High purity Al foil (thickness = 0.5 mm, purity = 99.999%) was obtained from the Beijing Trillion Metals Co., Ltd (Beijing, China). 4-Mercaptopyridine (4-MPy, 96%) was obtained from Sigma-Aldrich. Ethanol, silver nitrate (AgNO₃, \geq 99.8%), trisodium citrate (Na₃C₆H₅O·2H₂O, TSC, \geq 99.5%), HNO₃ (65%), and NaF (\geq 99.0%) were purchased from the Sinopharm Chemical Reagent Co., Ltd., (Shanghai, China). Ultrapure water with a resistivity greater than $18 \,\mathrm{M}\Omega \cdot \mathrm{cm}^{-1}$ was used throughout the present study. All the reagents were used as received without further purification.

2.2 Preparation of substrates

First, Al foil $(1 \text{ cm} \times 1 \text{ cm})$ was polished with sandpaper (500 meshes) and sonicated with water for 3 min. Next, Al foil was washed with water and dried by N₂ flow. The fabrication process of Ag nanosheets is shown in Scheme 1.



Scheme 1: Schematic illustration of preparation process of Ag nanosheets assembled on Al foil.

(1) Al foil was put into a vessel. (2) 0.8 mL mixed solution contained 30 mM NaF and 15 mM HNO₃ (NaF/HNO₃) were put into the vessel. The clean Al foil was immersed in NaF/HNO₃ etching solution for 1 min. (3) After that, 1.7 mL mixed solution containing 30 mM AgNO₃ and 3 mM TSC were added into the vessel, and the timing was started. After the expected reaction time, Al foil was removed from the reaction mixture, rinsed with water, and dried with N₂. The above experiment was conducted in a fume hood. The surface of the Al foil was covered by Ag nanosheets.

The Al foils covered with Ag nanosheets were used as SERS-active substrates. The substrates were immersed in 4-MPy ethanol solution (10⁻⁶ M) for 2 h and washed with ethanol and dried by N2 flow for further use.

2.3 Characterization

The morphologies were characterized using scanning electron microscopy (SEM, JEOL FESEM 6700F) with an accelerating voltage of 3 kV. The structures were characterized using transmission electron microscopy (TEM,

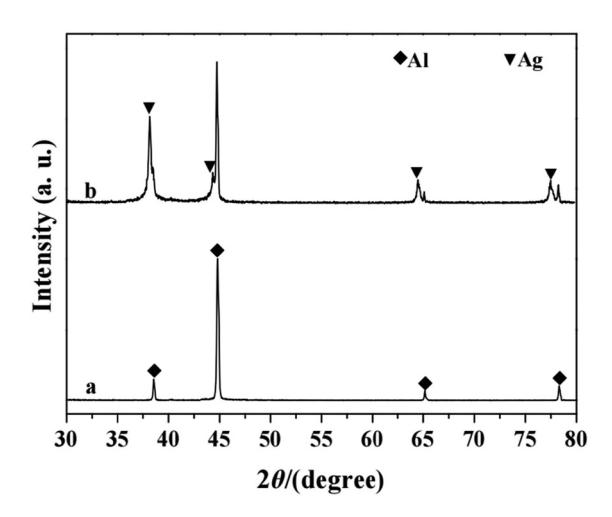


Figure 1: XRD Patterns of the products obtained at (a) 0 s and (b) 60 min.

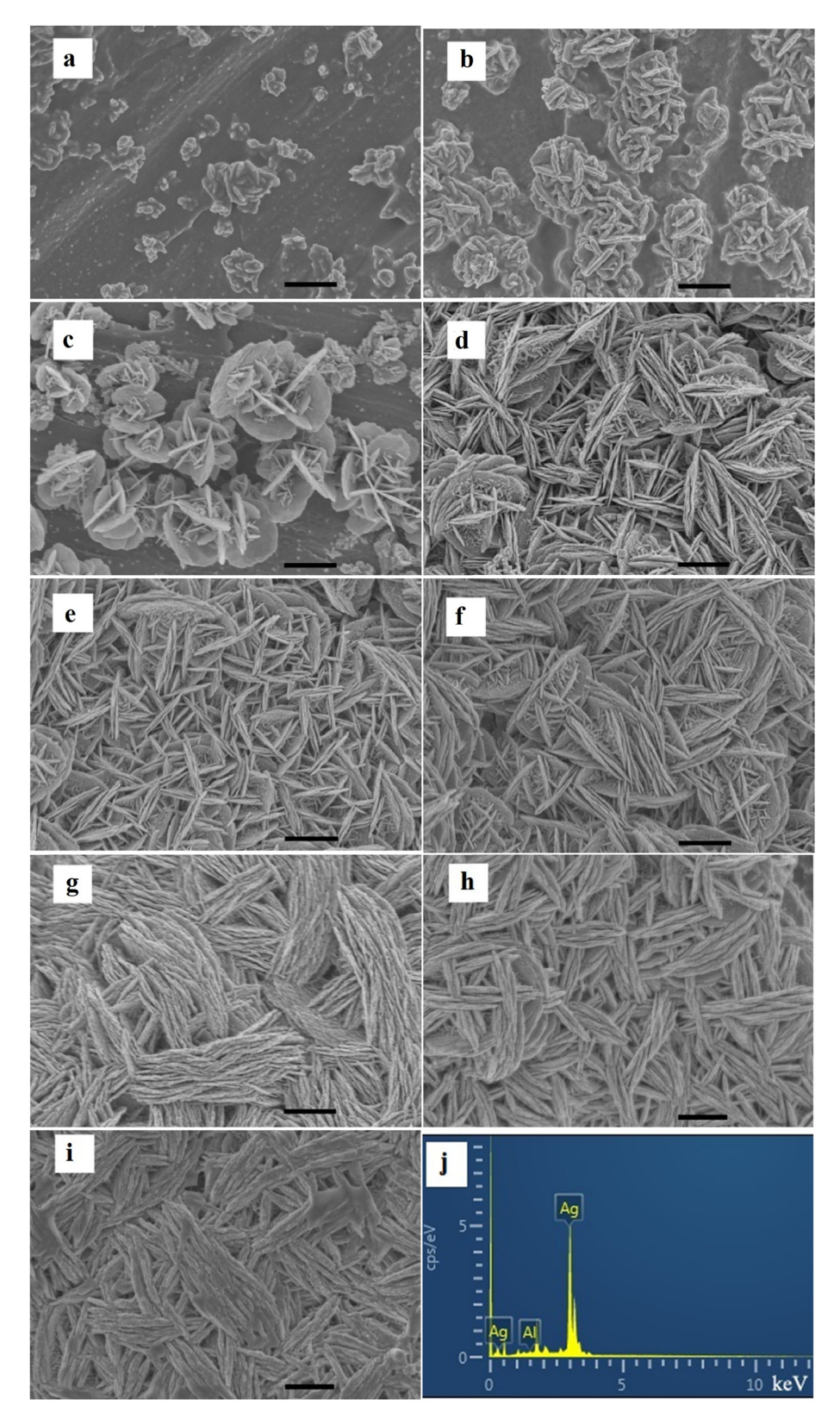


Figure 2: SEM Images of the products obtained at different reaction time: (a) 5 s, (b) 30 s, (c) 60 s, (d) 5 min, (e) 15 min, (f) 30 min, (g) 60 min, (h) 1.5 h, (i) 2.0 h, and (j) EDS spectrum of Ag shown in Figure 2g. The scale bar is $1 \mu m$.

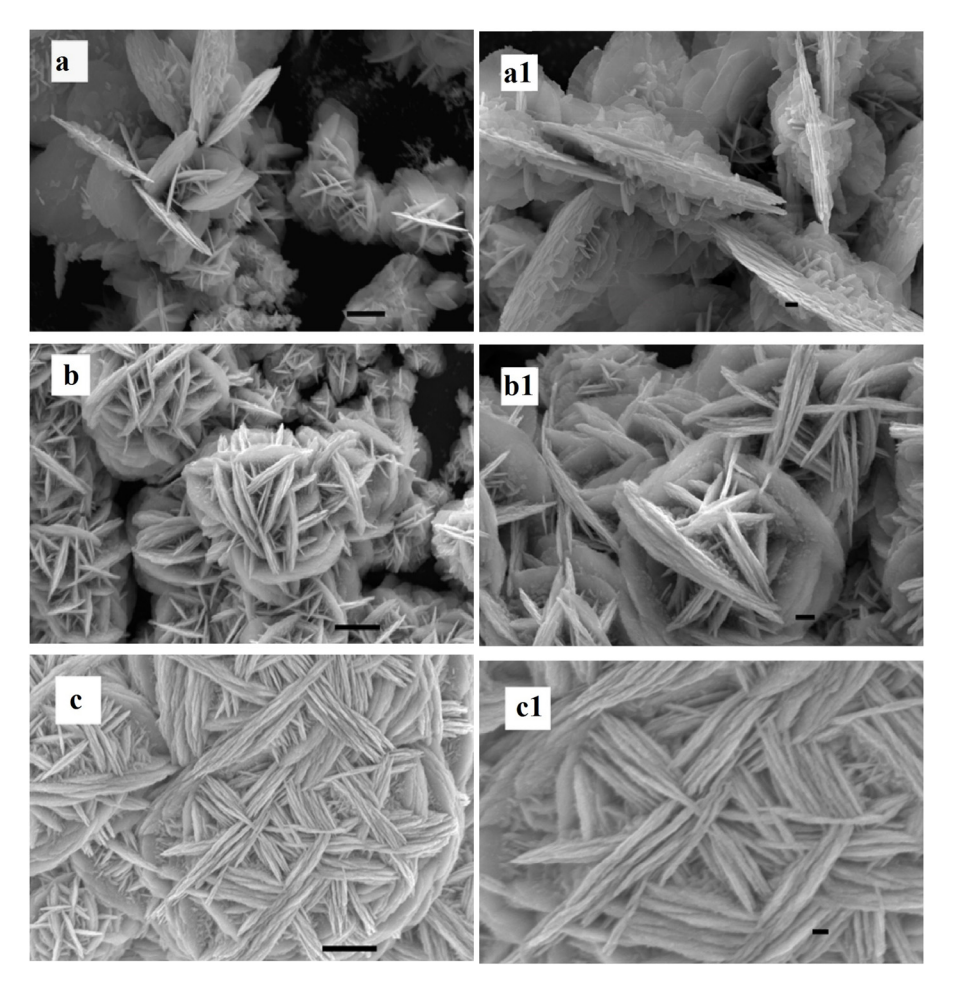


Figure 3: SEM Images of the products obtained at different concentrations of $AgNO_3$: (a) 10, (b) 20, and (c) 40 mM, the reaction time was 30 min (scale bar, $1 \mu m$), and (a1–c1) their corresponding magnified images (scale bar, 200 nm).

Hitachi H-800) at an accelerating voltage of 200 kV. X-ray diffraction (XRD) experiments were conducted using a Rigaku D/max 2500/PC diffractometer with Cu-K α radiation (λ = 1.5418 A). The SERS spectra were recorded with a Renishaw 1000 model Raman spectrometer. The radiation from an air-cooled argon-ion laser (532 nm) was used as an excitation source. The spot of the laser was a circle with a diameter of 1 μ m.

3 Results and discussion

3.1 Influence of the reaction time on the morphology

The phase structure of Al foils was characterized before and after the reaction by XRD. Curve a in Figure 1 shows the typical diffraction peaks of the Al according to JCPDS No. 65-2869. After Al reacted with Ag⁺, the XRD patterns

of the products were exhibited in curve b in Figure 1. With the increase of reaction time, the peaks from Ag indicate that the Ag is deposited on Al foils. These peaks of Ag with face-centered cubic structure come from the index (111), (200), (220), and (311) (JCPDS No. 04-0783) from left to right.

Figure A1 (in Appendix) shows the rough surface of Al foil before and after treatment with NaF and HNO₃. Time-dependent experiments were conducted to understand the formation process of Ag nanosheets. The SEM images in Figure 2 and their corresponding magnified images (Figure A2) present the morphologies of Ag nanosheets that assembled on Al foils at different reaction times. When Al foil reacted with Ag⁺ for 5 s, some Ag islands appeared on the surface of Al foil, as shown in Figure 2a. With further observation, it was found that the islands were composed of small nanoparticles and ridge-like protuberances (Figure A2a). These ridge-like protuberances were actually rudimentary nanosheets. Previous experiments had revealed the shape-controlling

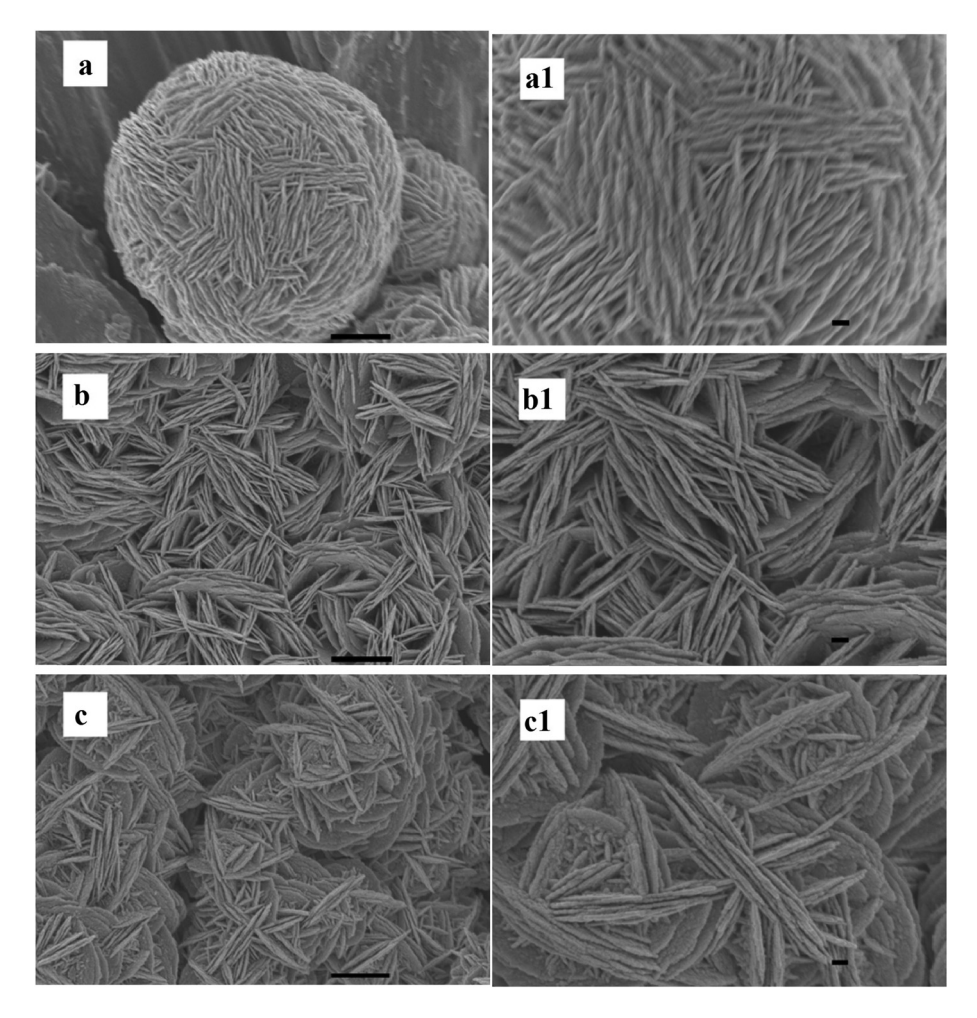


Figure 4: SEM Images of the products obtained at different concentrations of NaF/HNO₃: (a) 0, (b) 20/10, (c) 40/20 mM, the reaction time was 30 min (scale bar, $1 \mu m$), and (a1-c1) their corresponding magnified images (scale bar, 200 nm).

role of citrate ions on nanosheets [32,35]. In the initial stage of the reaction, small Ag nanoparticles were formed, which acted as nuclei for mediating the growth of nanosheets. At the same time, citrate ions were adsorbed on the {111} facets of the Ag nanoparticle and restricted the growth of this plane. With the prolonging of reaction time, Ag nuclei were formed into nanosheets [32,35,36]. As shown in Figure 2b and Figure A2b, the nanosheets had taken shape after the reaction time of 30 s. The figures demonstrated that the surfaces of the nanosheets were very rough, and small nanoparticles could be seen on them. Obviously, with the reaction going on, as the nanosheets continued to grow, these small nanoparticles would develop into the nanosheets under the influence of citrate ions. It could be verified in Figure 2c and Figure A2c. On large nanosheets, there are small nanosheets besides small nanoparticles. With the longer reaction time, the nanoparticles were constantly generated and developed into nanosheets. As a result, the nanosheets were bigger and increasing in number at the same time. So, the nanosheets

were connected in a parallel and intersection manner when the reaction time was long enough (Figure 2d–i and Figure A2d–i). There were sub-10 nm gaps formed between the adjacent nanosheets assembled in parallel as the black arrows marked in Figure A2d–i. When the reaction time was 1 h, the nanosheets were mainly assembled in parallel and filled almost all the voids. This would directly lead to the remarkable increase of sub-10 nm gaps. And, when the reaction time exceeded 1 h, the gaps were reduced dramatically, especially for 2.0 h (Figure 2h and i and Figure A2h and i). This was mainly due to the increase of nanosheets, which led to their fusion. Its EDS spectrum is presented in Figure 2j.

In addition, a supplementary experiment was performed in this work (Figure A3). When there is no TSC in the reaction solution, the Ag nanostructures on Al foil were composed of dendrites. This dramatic difference in the morphology from Figure 2a–i strongly suggested that citrate ions played a decisive role in the growth process of

Ag nanosheets. The scraped Ag nanosheets were ultrasonicated in ethanol, dripped onto a copper grid, and characterized by TEM. Sheet-like samples were presented in Figure A4.

3.2 Influence of AgNO₃ concentration on the morphology

In this work, the influence of the AgNO₃ concentration on the morphology of the products was investigated. The concentration of AgNO3 was respectively 10, 20, and 40 mM while keeping the other conditions unchanged. It was found that the morphology of the Ag products strongly depended on the concentrations of AgNO3 in the solution (Figure 3). At the low concentration of AgNO₃ such as 10 mM, even though the reaction time was as long as 30 min, the nanosheets were not enough to effectively cover Al foil (Figures 3a and a1). In contrast, at 20 and 40 mM concentration of AgNO₃ in the solution, the nanosheets were densely assembled (Figure 3b and c and b1 and c1). Even the voids surrounded by the bigger nanosheets are almost filled by smaller nanosheets and nanoparticles. We suggest that the reason for this is the effect of AgNO₃ concentration on the number of Ag nuclei at the primary and their subsequent growth stage [32,35]. Therefore, with the increase of AgNO₃ concentration, the density of nanosheets, especially nanosheets assembled in parallel, was significantly increased.

3.3 Influence of the NaF/HNO₃ concentration on the morphology

The influence of NaF/HNO₃ on the morphology of the products was investigated through varying NaF/HNO₃ concentration while keeping the other conditions unchanged. The experimental results are shown in Figure 4. When NaF and HNO₃ in the solution were 0 mM, a few scattered Ag nanoflowers composed with the nanosheets were formed (Figure 4a). In the absence of NaF and HNO₃, Al is easily oxidized to Al₂O₃ in solution according to the reaction in Eq. 1 as previously mentioned [22,26]. Al₂O₃ could hamper sufficient contact of Ag⁺ and Al, so the amount of Ag nuclei was very small at the primary stage, and the coverage density of the resulting nanosheets was very low. When the concentration of NaF/HNO₃ was increased to 20/10 and 40/20 mM, a large number of nanosheets were covered on the Al foils (Figure 4b and c). Besides, it was found that lots of the

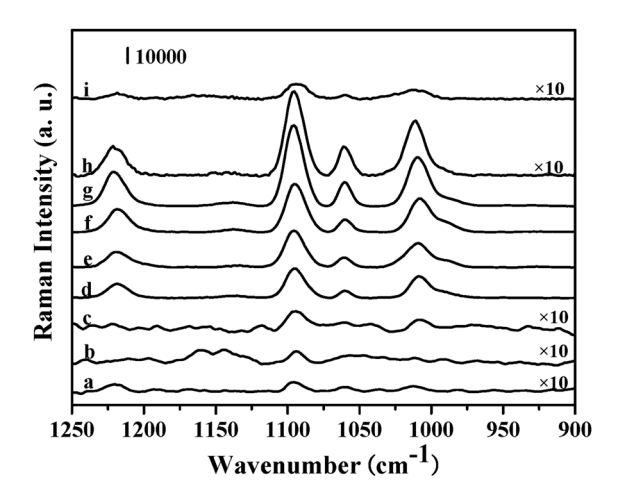
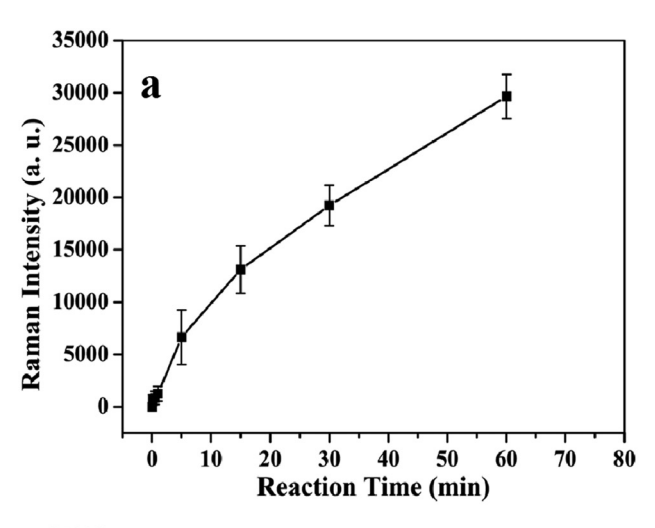


Figure 5: SERS Spectra of 4-MPy (10^{-6} M) adsorbed on the substrates with different morphologies shown in Figure 2a-i, respectively.

nanoparticles and the tiny nanosheets are on the side of the bigger nanosheets (Figures 4c and c1). The reason could be ascribed to the fact that HNO₃ at high concentration resulted in the etching and roughening of the surface of Ag nanosheets. So, the nanoparticles and the tiny nanosheets were constantly formed on the side of the nanosheets. The obtained experiment proves that the difference in the density of nanosheets reflected the important role of NaF and HNO₃ in the reaction.

3.4 SERS properties

Figure 5 shows SERS spectra of 4-MPy adsorbed on the substrates presented in Figure 2. The assignment of the peaks can be seen in the previous work [37]. As seen in Figure 5, the SERS intensity of 4-MPy first increased and then decreased with the reaction time (curves a-i). For clearer insight into the change of SERS intensity, the dependence of peak intensity at 1,010 cm⁻¹ with the reaction time was exhibited in Figure 6a. In the initial stage of the reaction, the nanosheets were only increased in number and arranged randomly on the Al foils. The nanosheets can generate strong electromagnetic fields at their edges and tips, and then enhance Raman signals [38–40]. Thus, the SERS signal intensity of the nanosheets fabricated within 0-1 min mostly depended on the number of the nanosheets. However, after 5 min, the new nanosheets were mainly assembled in parallel and increased with the reaction time. The parallel nanosheets provide sub-10 nm gaps as hot spots. The local electromagnetic field can reach huge values at the hot spots. And the presence of the hot



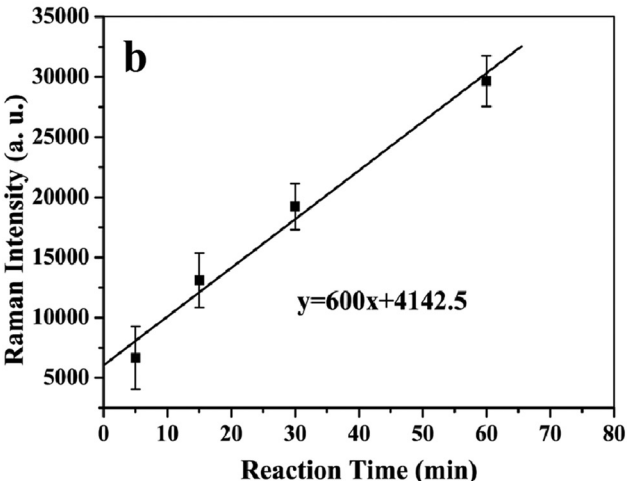


Figure 6: (a) The relationship of SERS intensity of 4-MPy at $1,010~\rm{cm^{-1}}$ and reaction time. (b) The linear relationship of SERS intensity of 4-MPy at $1,010~\rm{cm^{-1}}$ and reaction time.

spots can make a great contribution to SERS [32,34–36,41,42]. So, when the abscissa was 5 min, the intensity value showed a great jump, and there was an inflection point on the curve. When the reaction time reached 60 min, a new inflection point appeared. After that, the SERS intensity was sharply reduced. This was because the sub-10 gaps on the substrates were sharply reduced. During the reaction period of 5–60 min, the SERS intensity had shown a linear correlation with the reaction time. The linear correlation is shown in Figure 6b and Eq. 5:

$$y = 600x + 4142.5, (5)$$

where y is the peak intensity of the SERS spectra of 4-MPy at 1,010 cm⁻¹, and x is the time of galvanic replacement reaction. Enhancement factor (EF) of Ag nanosheets in Figure 2g was used to evaluate SERS enhancement ability. The calculative process for EF was presented in ESI. EF of the substrate was 3×10^5 .

4 Conclusions

In summary, Ag nanosheets with controlled morphology were prepared by the galvanic displacement reaction. Ag nanosheets were developed from Ag nuclei, and different reaction conditions influenced the number of Ag nuclei in the initial and subsequent growth stages. It can be found that the appropriate reaction conditions such as reaction time, reactant concentration became the key to control the density of silver nanosheets. TSC was employed as the shape controlling agent to ensure that Ag nuclei grew into the nanosheets. The high-density parallel nanosheets were ideal SERS substrates because they provided more sub-10 gaps as hot spots. This current study proves that the commercially available Ag, the simple synthetic way, and good enhancement ability will be helpful for expanding the prospects of large-scale synthetic Ag nanosheets SERS-based highly sensitive analysis.

Funding information: This research was supported by the Natural Science Foundation Project of Jilin Province (grant number YDZJ202201ZYTS425).

Author contributions: Yuhai Wang performed research, analyzed data, and wrote the paper; Chunxu Wang designed research and analyzed data; Yongling Zhang analyzed data and revised the manuscript; Jia Wang provided instrumentation, reagents, materials; Li Wang revised the manuscript.

Conflict of interest: The authors state no conflict of interest.

References

- Pieczonka NPW, Aroca RF. Single molecule analysis by surfaced-enhanced Raman scattering. Chem Soc Rev. 2008;37:946–54. doi: 10.1039/b709739p.
- [2] Han XX, Chen L, Ji W, Xie YF, Zhao B, Ozaki Y. Label-free indirect immunoassay using an avidin induced surfaceenhanced raman scattering substrate. Small. 2011;7(3):316–20. doi: 10.1002/smll.201001936.
- [3] Hering K, Cialla D, Ackermann K, Dörfer T, Möller R, Schneidewind H, et al. SERS: a versatile tool in chemical and biochemical diagnostics. Ana Bio Chem. 2008;;390(1):113–24. doi: 10.1007/s00216-007-1667-3.
- [4] Chen L, Zhao Y, Wang YX, Zhang YJ, Liu Y, Han XX, et al. Mercury species induced frequency-shift of molecular orientational transformation based on SERS. Analyst. 2016;141(15):4782-8. doi: 10.1039/C6AN00945J.
- [5] Wang L, Qi H, Chen L, Sun YT, Li Z. Self-assembled Ag-Cu₂O nanocomposite films at air-liquid interfaces for surface-

- enhanced Raman scattering and electrochemical detection of H₂O₂. Nanomaterials. 2018;8(5):332. doi: 10.3390/ nano8050332.
- [6] Zhang LX, Lian WH, Li P, Ma H, Han XX, Zhao B, et al. Crocein orange G mediated detection and modulation of amyloid fibrillation revealed by surface-enhanced Raman spectroscopy. Biosens Bioelectron. 2020;148:111816. doi: 10.1016/ i.bios.2019.111816.
- Kutsanedzie FYH, Agyekum AA, Annavaram V, Chen Q. Signalenhanced SERS-sensors of CAR-PLS and GA-PLS coupled AgNPs for ochratoxin A and aflatoxin B1 detection. Food Chem. 2020;315:126231. doi: 10.1016/j.foodchem.2020.126231.
- Ward DR, Grady NK, Levin CS, Halas NJ, Wu Y, Nordlander P, et al. Electromigrated nanoscale gaps for surface-enhanced Raman spectroscopy. Nano Lett. 2007;7(5):1396-1400. doi: 10.1021/nl070625w.
- Cecchini MP, Turek VA, Paget J, Kornyshev AA, Edel JB. Selfassembled nanoparticle arrays for multiphase trace analyte detection. Nat Mater. 2013;12:165-71. doi: 10.1038/ NMAT3488.
- [10] Kneipp K, Wang Y, Kneipp H, Perelman LT, Itzkan I, Dasari RR, et al. Single molecule detection using surface-enhanced raman scattering (SERS. Phys Rev Lett. 1997;78(3):1667-70. doi: 10.1103/PhysRevLett.78.1667.
- [11] Nie SM, Emory SR. Probing single molecules and single nanoparticles by surface-enhanced Raman scattering. Science. 1997;275(5303):1102-6. doi: 10.1126/ science.275.5303.1102.
- [12] Li L, Steiner U, Mahajan S. Single nanoparticle SERS probes of ion intercalation in metal-oxide electrodes. Nano Lett. 2014;14(2):495-8. doi: 10.1021/nl403485e.
- [13] Fleischmann M, Hendra PJ, McQuillan AJ. Raman spectra of pyridine adsorbed at a silver electrode. Chem Phys Lett. 1974;26(2):163-6. doi: 10.1016/0009-2614(74)85388-1.
- [14] Tian ZQ, Ren B, Wu DY. Surface enhanced Raman scattering: from noble to transition metals and from rough surfaces to ordered nanostructures. J Phys Chem B. 2002;106(37):9463-83. doi: 10.1021/jp0257449.
- [15] Tang LL, Liu Y, Chen GQ, Li QQ, Shi YY, Liu LL, et al. A novel SERS substrate platform: spatially stacking plasmonic hotspots films. Nanoscale Res Lett. 2019;14:94. doi: 10.1186/ s11671-019-2928-8.
- [16] Khlebtsov BN, Khanadeev VA, Panfilova EV, Bratashov DN, Khlebtsov NG. Gold nanoisland films as reproducible SERS substrates for highly sensitive detection of fungicides. ACS Appl Mater Inter. 2015;7(12):6518-29. doi: 10.1021/ acsami.5b01652.
- [17] Hu XG, Cheng WL, Wang T, Wang YL, Wang EK, Dong SJ. Fabrication, characterization, and application in SERS of selfassembled polyelectrolyte-gold nanorod multilayered films. J Phys Chem B. 2005;109(41):19385-9. doi: 10.1021/jp052706r.
- [18] Guo HY, Jiang D, Li HB, Xu SP, Xu WQ. Highly efficient construction of silver nanosphere dimers on poly(dimethylsiloxane) sheets for surface-enhanced Raman scattering. J Phys Chem C. 2014;117(1):564-70. doi: 10.1021/jp309396x.
- [19] Dick LA, McFarland AD, Haynes CL, Van Duyne RP. Metal film over nanosphere (MFON) electrodes for surface-enhanced Raman spectroscopy (SERS): improvements in surface nanostructure stability and suppression of irreversible loss. J Phys Chem B. 2002;106(4):853-60. doi: 10.1021/jp013638l.

- [20] Li XL, Xu WQ, Zhang JH, Jia HY, Yang B, Zhao B, et al. Selfassembled metal colloid films: two approaches for preparing new sers active substrates. Langmuir. 2004;20(4):1298-1304. doi: 10.1021/la0356396.
- [21] Wang KQ, Sun DW, Pu HB, Wei QY. Two-dimensional Au@Ag nanodot array for sensing dual-fungicides in fruit juices with surface-enhanced Raman spectroscopy technique. Food Chem. 2019;310(3):125923. doi: 10.1016/ j.foodchem.2019.125923.
- [22] Ye WC, Chen Y, Zhou F, Wang CM, Li YM. Fluoride-assisted galvanic replacement synthesis of Ag and Au dendrites on aluminum foil with enhanced SERS and catalytic activities. J Mater Chem. 2012;22:18327-34. doi: 10.1039/ C2IM32170I.
- [23] Sun YG, Mayers BT, Xia YN. Template-engaged replacement reaction: a one-step approach to the large-scale synthesis of metal nanostructures with hollow interiors. Nano Lett. 2002;2(5):481-5. doi: 10.1021/nl025531v.
- [24] Zhuo K, An CY, Kannan PK, Seo N, Park YS, Chung CH. Effect of electrolyte composition on the morphological structures of dendritic copper powders prepared by a spontaneous galvanic displacement reaction. Korean J Chem Eng. 2017;34:1483-9. doi: 10.1007/s11814-017-0023-3.
- [25] Xie SP, Zhang XC, Yang SL, Paau MC, Xiao D, Choi MMF. Liesegang rings of dendritic silver crystals emerging from galvanic displacement reaction in a liquid-phase solution. RSC Adv. 2012;2:4627-31. doi: 10.1039/C2RA20055D.
- [26] Ou JF, Shi QW, Chen YW, Wang FJ, Xue MS, Li W. Superhydrophobic surfaces on diverse metals based on ultrafastsequential deposition of silver and stearic acid. Appl Surf Sci. 2015;326:139-44. doi: 10.1016/ j.apsusc.2014.11.107.
- [27] You HJ, Chen F, Yang SC, Yang ZM, Ding BJ, Liang SH, et al. Size Effect on Nanoparticle-Mediated Silver. Cryst Growth Des. 2011;13(6):2696. doi: 10.1021/cg400573n.
- [28] Gutés A, Carraro C, Maboudian R. Silver dendrites from galvanic displacement on commercial aluminum foil as an effective SERS substrate. J Am Chem Soc. 2010;132:1476-7. doi: 10.1021/ja909806t.
- [29] Xie SP, Zhang XC, Xiao D, Paau MC, Choi MMF. Fast growth synthesis of silver dendrite crystals assisted by sulfate ion and its application for surface-enhanced Raman scattering. J Phys Chem C. 2011;115(20):9943-51. doi: 10.1021/jp201484r.
- [30] Jie Z, Meng G, Zhu C, Zhou Q, Li Z, Yan K, et al. Ordered arrays of Ag nanodendrite clusters as effective surface-enhanced Raman scattering substrates. Rsc Adv. 2016;6:26490-4. doi: 10.1039/C6RA03223K.
- Li XX, Lin X, Liu BK, Zhao XL, Zhao HY, Wang L, et al. Citrate-assisted galvanic replacement for fabrication of homogeneous Ag nanosheets as high-performance SERS substrate. Appl Phys A. 2019;125:492. doi: 10.1007/s00339-019-2786-3.
- [32] Gao T, Wang YQ, Wang K, Zhang X, Dui J, Li G, et al. Controlled synthesis of homogeneous Ag nanosheet-assembled film for effective SERS substrate. ACS Appl Mater Interfaces. 2013;5(15):7308-14. doi: 10.1021/am401552x.
- [33] Li ZB, Meng GW, Liang T, Zhang Z, Zhu XG. Facile synthesis of large-scale Ag nanosheet-assembled films with sub-10 nm gaps as highly active and homogeneous SERS substrates. Appl Surf Sci. 2013;264:383-90. doi: 10.1016/j.apsusc.2012.10.031.

- [34] Liu GQ, Cai WP, Liang CH. Trapeziform Ag nanosheet arrays induced by electrochemical deposition on Au-coated substrate. Cryst Growth Des. 2008;8(8):2748-52. doi: 10.1021/ cg700933p.
- [35] Wang YQ, Wang K, Zou BF, Gao T, Zhang XL, Du ZL, et al. Magnetic-based silver composite microspheres with nanosheet-assembled shell for effective SERS substrate. J Mater Chem C. 2013;1:2441-7. doi: 10.1039/C3TC30106K.
- [36] Zhang B, Xu P, Xie XM, Wei H, Li ZP, Mack NH, et al. Aciddirected synthesis of SERS-active hierarchical assemblies of silver nanostructures. J Mater Chem. 2011;21:2495. doi: 10.1039/c0jm02837a.
- [37] Ji N, Ruan WD, Wang CX, Lv ZC, Zhao B. Fabrication of silver decorated anodic aluminum oxide substrate and its optical properties on surface-enhanced Raman scattering and thin film interference. Langmuir. 2009;25(19):11869-73. doi: 10.1021/la901521j.

- [38] Zou X, Dong S. Surface-enhanced Raman scattering studies on aggregated silver nanoplates in aqueous solution. J Phys Chem B. 2006;110(43):21545-50. doi: 10.1021/jp063630h.
- [39] Pastoriza-Santos I, Liz-Marzán LM. Colloidal silver nanoplates. State of the art and future challenges. J Mater Chem. 2008;18:1724-37. doi: 10.1039/b716538b.
- [40] Kelly KL, Coronado E, Zhao LL, Schatz GC. The optical properties of metal nanoparticles: the influence of size, shape, and dielectric environment. J Phys Chem. 2003;107(3):668-77. doi: 10.1021/jp026731y.
- [41] Xu W, Meng G, Huang Q, Hu X, Huang Z, Tang H, et al. Largescale uniform Ag-NW tip array with enriched sub-10-nm gaps as SERS substrate for rapid determination of trace PCB77. Appl Surf Sci. 2013;271:125-30. doi: 10.1016/j.apsusc.2013.01.144.
- [42] Wang H, Levin CS, Halas NJ. Nanosphere arrays with controlled sub-10-nm gaps as surface-enhanced Raman spectroscopy substrates. J Am Chem Soc. 2005;127(43):14992-3. doi: 10.1021/ja055633y.

Appendix

The calculative process for EF [37]:

$$EF = \frac{I_{SERS}/N_{Surf}}{I_{RS}/N_{Vol}}$$
 (A1)

where $N_{\rm Vol} = c_{\rm RS}V$ is the average number of molecules in the scattering volume (V) for the Raman (non-SERS) measurement and $N_{\rm Surf}$ is the average number of adsorbed molecules in the scattering volume for the SERS experiments. Herein, 50 μ L of 4-MPy in ethanol (10^{-6} M) disperse on Al foil ($1\,{\rm cm}\times 1\,{\rm cm}$). An assumption is made that 4-MPy is absorbed on the substrate as a homogeneous monolayer, and then, the average area occupied by each 4-MPy is estimated to be $3.3\,{\rm nm}^2$. The result is

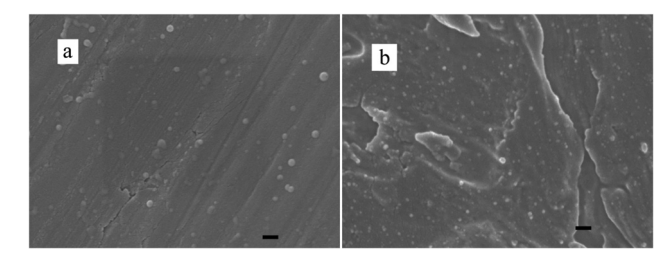


Figure A1: SEM images of Al foils (a) before and (b) after treatment with NaF and HNO₃ (scale bar, 200 nm).

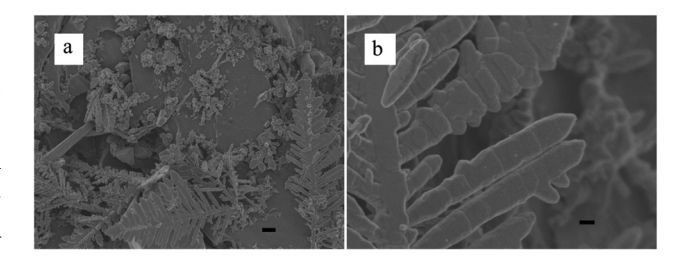


Figure A3: (a) SEM images of the products obtained at TSC 0 mM (scale bar, $1 \mu m$) and (b) its corresponding magnified images (scale bar, 200 nm).

enormously larger than the reported unimolecular area of $0.18~\text{nm}^2$ of 4-MPy absorbed on Ag. So, 4-MPy is absorbed on substrates as a sub-monolayer. The spot of the laser is a circle with a diameter of 1 μ m. N_{Surf} can be calculated to be 2.36×10^7 . The reference used in non-SERS measurement is 0.3~M 4-MPy in ethanol. For the optical configuration and microscope employed here, the effective focused depth is $21~\mu$ m, so $N_{\text{Vol}} = c_{\text{RS}}V$ is about 3×10^9 . Figure A4 shows the Raman and SERS spectra of 4-MPy in solution and on substrates presented in Figure 2h, respectively. For the vibration mode at 1,010 cm⁻¹, $I_{\text{SERS}}/I_{\text{RS}}$ is 2,403 and EF of the substrate is 3×10^5 .

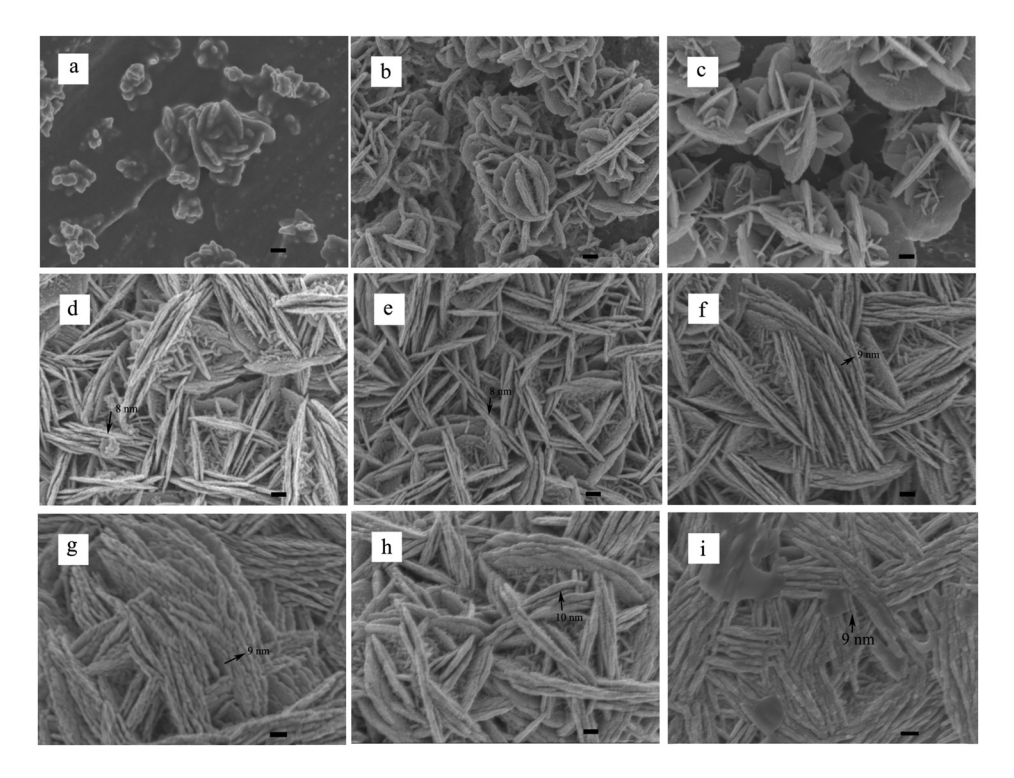


Figure A2: SEM images of the products obtained at different reaction time: (a) 5 s, (b) 30 s, (c) 60 s, (d) 5 min, (e) 15 min, (f) 30 min, (g) 60 min, (h) 1.5 h, and (i) 2 h (scale bar, 200 nm).

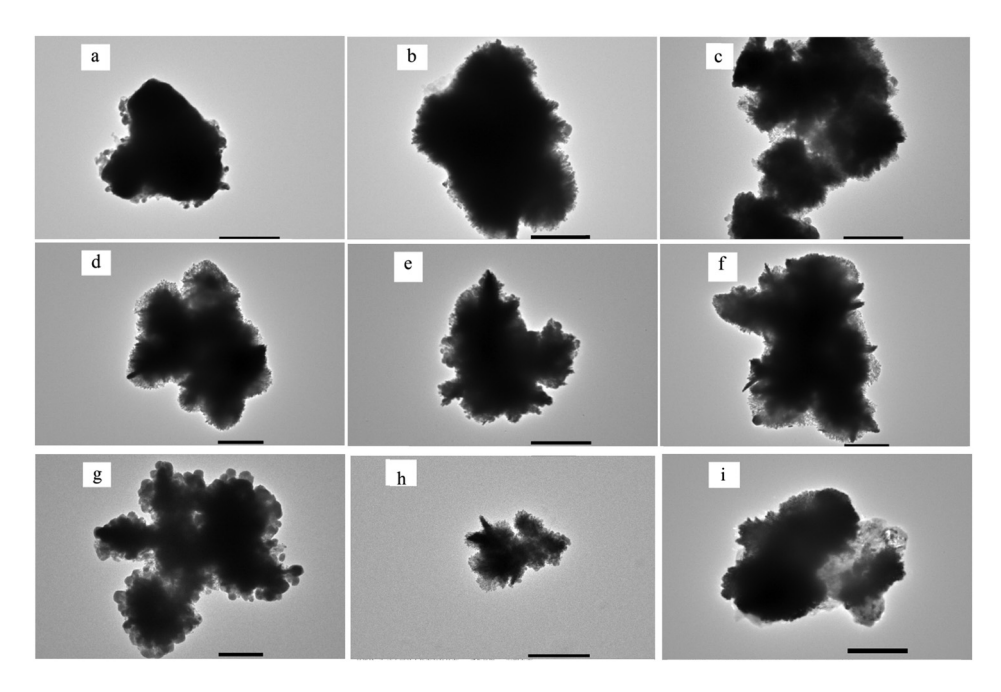


Figure A4: TEM image of a broken piece of the Ag nanosheets at different reaction time: (a) 5 s, (b) 30 s, (c) 60 s, (d) 5 min, (e) 15 min, (f) 30 min, (g) 60 min, (h) 1.5 h, and (i) 2 h (scale bar, 500 nm).

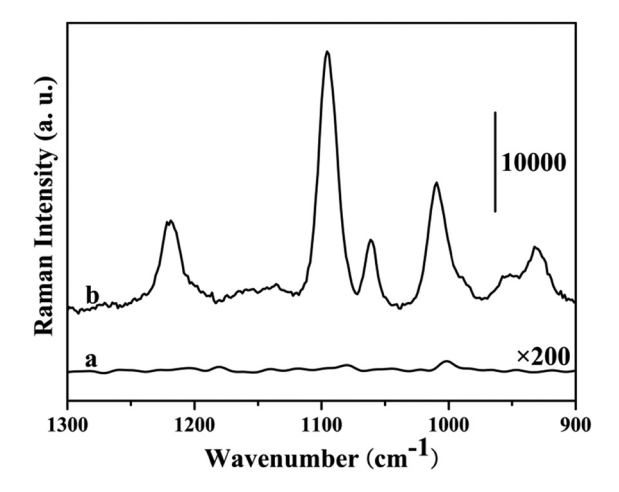


Figure A5: (a) Raman spectrum of 0.3 M 4-MPy in ethanol ($200 \times$ magnification) and (b) SERS spectrum of 10^{-6} M 4-MPy absorbed on the SERS substrate presented in Figure 2g.